MALAYSIAN JOURNAL OF MICROSCOPY

Journal homepage: https://malaysianjournalofmicroscopy.org

RESEARCH ARTICLE

CHEMICALLY ACTIVATED SUNFLOWER SEED SHELL BASED ACTIVATED CARBON FOR ALLOPURINOL REMOVAL: ISOTHERM, KINETICS AND REGENERATION STUDIES

Mohd Raziff Mat Hasan[1], Azrina Aziz[1], Erniza Mohd Johan Jaya[1], Mohd Azmier Ahmad[1,*]

[1]School of Chemical Engineering, Engineering Campus, Universiti Sains Malaysia, 14300 Nibong Tebal, Pulau Pinang, Malaysia.

Abstract. Allopurinol (ALP) is an emerging contaminant that enters aquatic environments due to incomplete removal in wastewater treatment plants. Its major metabolite, oxypurinol, can form riboside adducts through the purine metabolism pathway, potentially disrupting purine metabolism in aquatic organisms. This study aims to synthesize and evaluate sunflower seed shell-derived activated carbon (SSSAC) for the adsorption of ALP from aqueous solutions. The SSSAC was produced through chemical activation using potassium hydroxide (KOH). Scanning electron microscopy (SEM) revealed that the raw sunflower seed shells exhibited a dense and non-porous morphology, whereas the SSSAC displayed a well-developed porous texture. The zeta potential of the precursor was −33.00 mV, which decreased to −51.30 mV after KOH activation, indicating enhanced surface negativity. In batch adsorption studies, increasing the initial ALP concentration from 10 to 100 mg/L resulted in a rise in adsorption capacity from 9.11 to 74.37 mg/g, while the percentage removal declined from 91.10 % to 74.37 % at higher concentrations. The optimum pH for ALP adsorption was pH 5, achieving a maximum capacity of 87.54 mg/g. Isotherm study revealed that the Freundlich model best represented the adsorption behaviour, with the lowest root mean square error (RMSE) of 1.15 mg/g and an average error of 5.52 %, signifying a multilayer adsorption process. The Langmuir model predicted a maximum monolayer capacity (Q_m) of 113.84 mg/g. Kinetic analysis confirmed that adsorption followed the pseudo-first-order (PFO) model. Regeneration studies showed that SSSAC remained reusable up to five cycles, after which the ALP uptake declined to 34.53 mg/g and the adsorbent yield decreased to 50.24 %. These findings demonstrate that SSSAC is a promising low-cost adsorbent for the effective removal of ALP from contaminated water systems.

Keywords: Activated carbon, chemical activation, isotherm, kinetic, regeneration.

Article Info

Received 9 January 2026
Accepted 15 April 2026
Published 8 June 2026

***Corresponding author: chazmier@usm.my**

ISSN: 1823-7010, eISSN: 2600-7444

1. INTRODUCTION

Allopurinol (ALP, 1,5-dihydro-4H-pyrazolo[3,4-d]pyrimidin-4-one) is widely prescribed for chronic gout and hyperuricemia linked to leukaemia, radiotherapy, chemotherapy, and diuretic use [1]. As a structural isomer of hypoxanthine, ALP inhibits xanthine oxidase, blocking the conversion of hypoxanthine to xanthine and xanthine to uric acid. Since xanthine oxidase activity generates uric acid and reactive oxygen species that contribute to tissue damage, its inhibition alleviates gout and related complications. Consequently, xanthine oxidase inhibitors not only serve as effective anti-gout agents but also show potential in anticancer therapy. ALP is only partially metabolized in the human body, with a significant fraction excreted unchanged via urine. As a result, it enters municipal wastewater through domestic sewage [2]. Conventional wastewater treatment plants are often ineffective in fully removing such persistent pharmaceutical residues, allowing ALP to pass into surface waters and, ultimately, river systems. The concentration of ALP in water ranges from 0.01 to 0.6 µg/L [3] and can reach up to 233 µg/L [4]. Therefore, advanced wastewater treatment strategies are required to effectively degrade or adsorb allopurinol before its release into the aquatic environment.

Adsorption is widely applied for removing diverse pollutants, including pharmaceutical contaminants, due to its simplicity, efficiency, and cost-effectiveness [5]. Activated carbon (AC) remains the most common adsorbent. AC is a disordered carbonaceous solid with a network of fine pores that greatly increases its accessible surface. This extensive porosity provides active sites for adsorption and chemical transformations. Depending on preparation conditions, AC can possess internal surface areas between 300 and 2500 m^2/g and pore volumes in the range of 0.20–0.60 cm^3/g. However, the conventional route of producing AC from coal is associated with serious environmental drawbacks, including the depletion of non-renewable resources, greenhouse gas emissions, and disposal challenges linked to mining activities. In addition, coal-based production often incurs high operational costs, which further limits its long-term sustainability and economic viability. To address this, increasing attention is directed toward sustainable AC derived from agricultural by-products such as coconut shell [6], *Lansium parasiticum* trunk [7] and others. One of the methods to produce AC is via chemical activation. Chemical activation is one of the most adaptable and widely applied methods for controlling the pore structure and surface chemistry of AC [8]. In contrast to physical activation, it can be performed directly on raw precursors without requiring an initial carbonization stage. A sequential two-step route, where the biomass undergoes carbonization followed by impregnation with an activating agent, also provides certain advantages. The preliminary pores formed during carbonization improve the penetration and uniform distribution of the activating compounds within the carbon matrix. This method often produces AC of superior quality. The activation procedure typically begins with impregnation or mixing of the precursor with a chemical reagent such as alkaline agent or acidic agent at a specific ratio, followed by thermal treatment at temperatures between 400 °C and 1000 °C.

Basic chemical activators can be classified into three categories: powerful agents like hydroxides, intermediate compounds such as carbonates, and milder substances including silicates and some oxides. Within the strong category, potassium hydroxide (KOH) has proven to be the most efficient, producing activated carbons with remarkably large surface areas, often surpassing 2000 m^2/g, and with porosity dominated by micropore structures [8]. In this study, sunflower seed-shell was converted to AC (SSSAC) via chemical activation using KOH to adsorb ALP molecules in water. The edible oil sector generates large amounts of sunflower seed shell, which represent a significant lignocellulosic residue on a global scale. These hulls, often amounting to nearly half of the seed weight, are commonly underutilized, being discarded in open storage, used as landfill material, or simply incinerated [9]. Growing environmental challenges have encouraged the search for more sustainable management practices. One promising route is the thermal conversion of such agricultural residues into value-added products, including AC as adsorbent for wastewater treatment, offering both ecological benefits and economic opportunities. The objective of this study is to synthesize and characterize SSSAC derived from sunflower seed shells and to evaluate its effectiveness for the adsorption of ALP from aqueous solutions. The novelty of this study is in utilizing sunflower seed shell as a low-cost precursor for ALP removal, which has received limited attention compared to other pharmaceutical contaminants. The main contribution lies in systematically evaluating the adsorption performance,

isotherm, kinetics and reusability of SSSAC for ALP removal. However, the study is limited to batch-scale experiments, and further investigation under continuous flow systems is recommended to assess its applicability in real wastewater treatment scenarios.

2. MATERIALS AND METHODS

2.1 Precursor, chemicals and SSSAC synthesis

The raw material applied in this work was sunflower seed shell collected from Penang, Malaysia. Potassium hydroxide (KOH pellets, 85 % grade) was employed as the activating reagent and obtained from Sigma-Aldrich. High-purity nitrogen, N_2 gas (99.99 %) was supplied by MOX Gases Berhad, Malaysia. A 0.05 M sodium hydroxide solution was prepared from analytical-grade NaOH pellets (≥98 %, Sigma-Aldrich) and used for the regeneration experiments. Prior to use, the sunflower shell was repeatedly washed with distilled water and subsequently dried in an oven at 60 °C for about 48 hours. The cleaned biomass was then subjected to carbonization at 600 °C for 2 hours under a constant N_2 stream (150 cm^3/min), producing the char. Similar carbonization conditions under an inert N_2 atmosphere have been widely reported for the preparation of biomass-derived AC [10]. To maintain its stability and prevent oxidation, the char was allowed to cool while continuously purged with N_2. After cooling, impregnation with KOH was carried out for 24 hours at an impregnation ratio (IR) of 1.0 g/g, which is a commonly adopted chemical activation approach to enhance pore development in biomass-based AC. The IR was defined as the ratio of the weight of KOH to the weight of char, calculated according to the following equation [11] :

$$Impregnation\ ratio\ (IR) = \frac{W_{KOH}}{W_{char}} \quad (1)$$

where W_{KOH} represents the weight of KOH and W_{char} represents the weight of the char.

2.2 Characterization methods

The investigation carefully evaluated the physicochemical characteristics of the prepared samples, such as specific surface area measured by Brunauer–Emmett–Teller (BET) method, mesoporosity, pore volume, and pore diameter distribution. These textural properties were obtained using a Micromeritics ASAP 2010 adsorption–desorption analyser. The elemental make-up of the samples was analysed with a PerkinElmer Series II 2400 instrument (USA). Furthermore, surface features and structural patterns were visualized through scanning electron microscopy (SEM) performed on a Quanta 450 FEG system (Netherlands), providing high-resolution images of the material morphology.

2.3 Isotherm investigation

For the adsorption isotherm investigation, six distinct initial concentrations of ALP solution (C_0, mg/L) were prepared in individual Erlenmeyer flasks at concentrations of 10, 20, 40, 60, 80, and 100 mg/L. Each flask was subsequently placed in a thermostatic bath shaker operating at a constant agitation speed of 80 rpm to ensure proper mixing. Experimental parameters, including the working temperature of 30 °C, the weight of SSSAC adsorbent (W_{SSSAC}, 0.20 g), and the solution volume (V, 200 mL), were consistently maintained. After the system reached equilibrium, the concentration of ALP at equilibrium phase (C_e, mg/L) was determined by ultraviolet–visible spectroscopy using an Agilent Cary 60 instrument (USA). Finally, the equilibrium adsorption capacity (q_e, mg/g) was computed based on the mass balance relationship shown below, which describes the relationship between initial concentration, equilibrium concentration, solution volume, and the amount of adsorbent used [12]:

$$q_e = \frac{(C_o - C_e)V}{W_{SSSAC}} \quad (2)$$

Three adsorption isotherm models namely Langmuir, Freundlich, and Temkin were used to analyse the experimental results. Below are the related equations for each model:

Langmuir [13]:

$$q_e = \frac{Q_m K_L C_e}{1 + K_L C_e} \quad (3)$$

Freundlich [13]:

$$q_e = K_F C_e^{1/n_F} \quad (4)$$

Temkin [13]:

$$q_e = \frac{RT}{B} \ln(AC_e) \quad (5)$$

where Q_m (single layer capacity (mg/g)) and K_L (capacity-related constant (L/mg)) are Langmuir parameters; n_F (dimensionless factor of heterogeneity) and K_F (constant of Freundlich ((mg/g)(L/mg)$^{1/n}$)) are Freundlich parameters; B (L/mg) and A (L/mg) are Temkin parameters, R is the universal gas constant (8.314 J mol^{-1} K^{-1}) and T (K) is the absolute temperature [14].

2.4 Kinetic investigation

Experimental batch data were utilized to evaluate adsorption kinetics through two commonly applied modelling approaches, namely the pseudo-first-order (PFO) and pseudo-second-order (PSO) rate equations. These kinetic models were carefully assessed using the mathematical expressions provided below, enabling a thorough exploration of adsorption behaviour, rate-controlling steps, and potential diffusion influences. Such an assessment not only revealed valuable information on the interaction patterns between ALP molecules and the prepared adsorbent but also contributed to a more comprehensive interpretation of the kinetic pathways and controlling mechanisms that regulate the overall adsorption performance in aqueous systems:

PFO [15]:

$$q_t = q_e[1 - exp(-k_1 t)] \quad (6)$$

PSO [15]:

$$q_t = \frac{k_2 q_e^2 t}{1 + k_2 q_e t} \quad (7)$$

The parameters associated with these kinetic equations are described in detail in reference [14].

2.5 Regeneration investigation

The saturated SSSAC was regenerated using a combined solvent–alkaline treatment to promote efficient desorption of ALP molecules. Initially, the spent SSSAC was rinsed three times with an ethanol–water mixture (50 % v/v) at a solid-to-liquid ratio of 1:100 g/mL, each wash conducted for 20 min at 80 rpm. This step helped to remove loosely bound compounds through disruption of weak interactions. Subsequently, chemical regeneration was carried out by treating the material with 0.05 M

NaOH solution under continuous stirring (80 rpm) for 1 h. The regenerated adsorbent was thoroughly rinsed with deionized water until the effluent reached neutral pH, then dried at 70 °C until constant weight was achieved. For each regeneration cycle, adsorption experiments were repeated under identical conditions as the fresh system: solution volume (200 mL), initial concentration (100 mg/L ALP), and adsorbent mass (0.20 g of regenerated SSSAC, denoted as $SSSAC_n$, where n is the regeneration cycle number). The regeneration parameters were calculated as follows [16]:

$$Adsorption\ uptake, q_{e,n}\ \left(\frac{mg}{g}\right) = \frac{(C_o - C_{e,n})V}{m} \quad (8)$$

$$Regeneration\ efficiency, RE_n\ (\%) = \frac{q_{e,n}}{q_{e,fresh}} \times 100 \quad (9)$$

$$Weight\ loss_n\ (\%) = \frac{m_{fresh} - m_n}{m_{fresh}} \times 100 \quad (10)$$

where $C_{e,n}$ is the equilibrium concentration after cycle *n* (mg/L), $q_{e,n}$ is the adsorption uptakes after cycle *n* (mg/g), m_{fresh} is the original mass of SSSAC and m_n is the mass of SSSAC after cycle *n*.

3. RESULTS AND DISCUSSION

3.1 Characterization results of precursor, char and SSSAC

3.1.1 Characteristics of surface area and pores characteristic

Table 1 presents the surface area and pore textural properties of the precursor, char, and SSSAC. The precursor showed negligible porosity, with a BET surface area of only 1.59 m^2/g, indicating its limited adsorption potential in the raw form. Furthermore, no measurable mesoporous surface area, total pore volume, or average pore diameter was detected for the precursor, reflecting its highly compact and unmodified lignocellulosic structure. Upon carbonization, the char exhibited some degree of pore development, with BET surface area of 418.63 m^2/g, mesopores surface area of 298.63 m^2/g, total pore volume of 0.1625 cm^3/g and an average pore diameter of 1.87 nm, but the values remained low, highlighting that pyrolysis alone was insufficient to achieve extensive porosity. In contrast, the subsequent chemical activation step with KOH dramatically enhanced the porous framework of the material. The BET surface area increased to 891.73 m^2/g. Similarly, the mesopore surface area reached 646.86 m^2/g, with a total pore volume of 0.2514 cm^3/g and an enlarged average pore diameter of 2.29 nm, which lies in the mesoporous spectrum. This significant enhancement can be attributed to the synergistic action of the two-stage process. Initially, pyrolysis facilitates the volatilization of unstable components, opening primary pores in the carbon structure. Subsequently, KOH activation penetrates deeply into the carbon matrix. These reactions etch the carbon framework and create additional pore channels, simultaneously widening existing pores [14].

Table 1: Surface area and pore characteristics of samples

Samples	BET surface area (m^2/g)	Mesopores surface area (m^2/g)	Total pore volume (cm^3/g)	Average pore diameter (nm)
Precursor	1.59	-	-	-
Char	418.63	298.63	0.1625	1.87
SSSAC	891.73	646.86	0.2514	2.29

3.1.2 Surface morphology via SEM image

Figure 1 presents the scanning electron microscopy (SEM) images that depict the morphological evolution of the samples before and after activation. In Figure 1(a), the precursor surface appears compact, dense, and largely featureless, with no obvious pore channels visible. This morphology is characteristic of untreated lignocellulosic biomass, whose structural components, particularly lignin, restrict the development of open pores. The dense texture reflects the raw, unprocessed state of the material, which lacks significant pathways for fluid diffusion or adsorption. In sharp contrast, Figure 1(b) illustrates the striking transformation in surface morphology after the precursor was converted to SSSAC. The SSSAC exhibits a highly porous surface, with a profusion of well-developed voids and cavities (indicated by yellow circles) distributed across the SSSAC's surface. Such a drastic morphological change is the direct outcome of the combined carbonization and chemical activation steps. During carbonization, moisture and volatile compounds were released, leaving a basic porous carbon skeleton. Subsequent KOH activation further modified this framework, as the alkali penetrated and reacted with the carbon matrix to generate gases and potassium compounds that etched the structure [17]. This process created new pores and enlarged existing ones, producing the interconnected porous morphology observed in the SEM images of SSSAC.

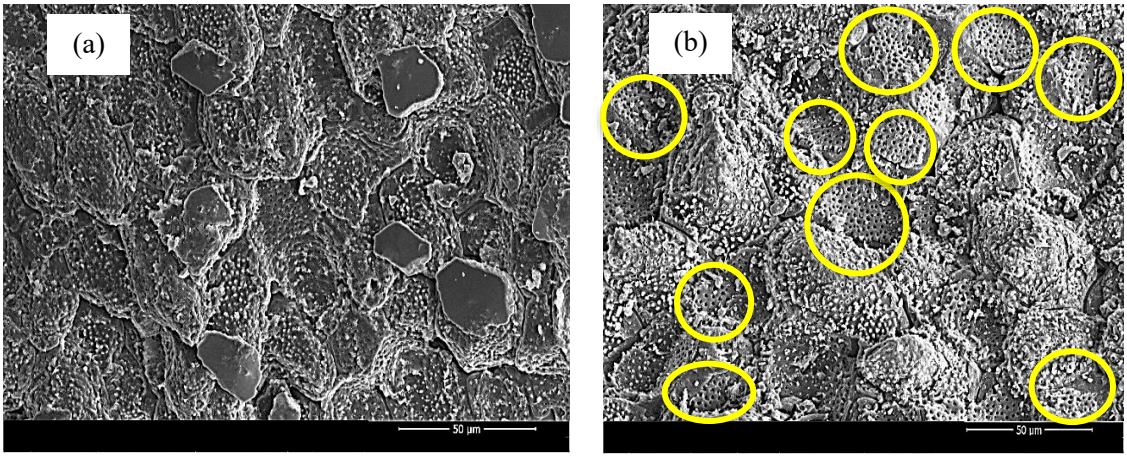

Figure 1: SEM images of (a) precursor and (b) SSSAC at magnification level of 1000×

3.1.3 Zeta potential readings

Figure 2 shows the zeta potential distributions for (a) the precursor and (b) the SSSAC. The precursor recorded a zeta potential of −33.00 mV, indicating a moderately negative surface charge. This negativity arises from oxygenated functional groups such as hydroxyl, carboxyl, and phenolic moieties naturally present in lignocellulosic biomass, which deprotonate in aqueous medium and contribute to surface charge. The value suggests a reasonably stable dispersion but with limited adsorption reactivity compared to AC. After KOH activation, the zeta potential of SSSAC decreased further to −51.30 mV, showing a stronger negative charge. This significant change reflects the chemical action of activation, where KOH etched the carbon framework, widened pores [11], and generated additional oxygenated functional groups, particularly phenol and carboxylic groups [18]. The increase in surface acidity results in higher anionic character, greater electrostatic repulsion between particles, and improved colloidal stability.

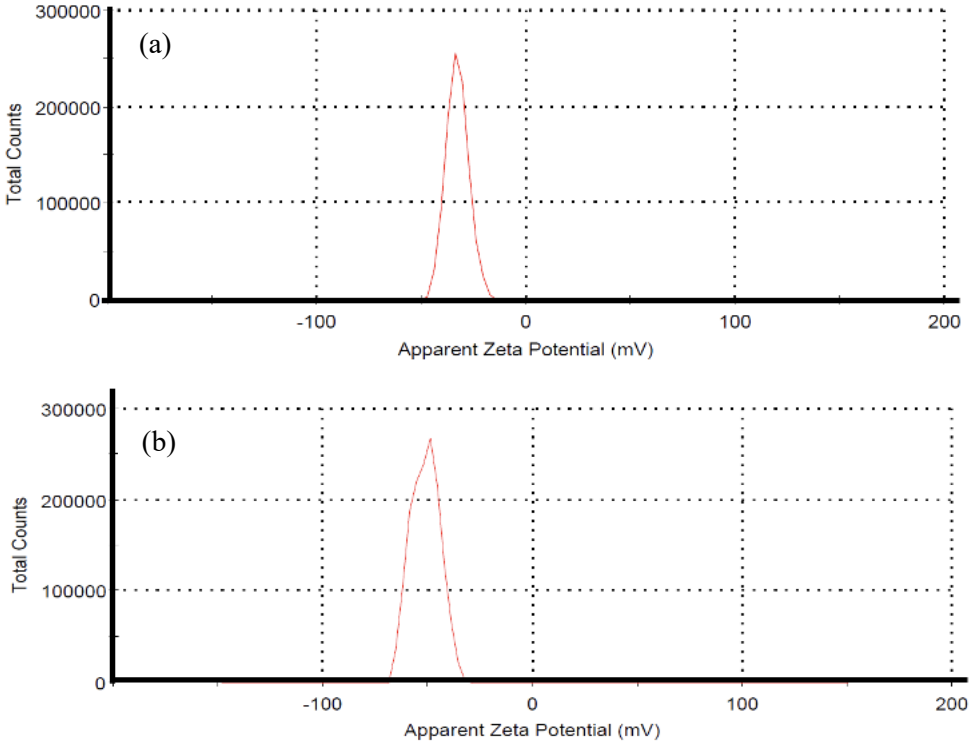

Figure 2: Zeta potential peak for (a) precursor and (b) SSSAC

3.2 Adsorption equilibrium

3.2.1 The influence of ALP starting concentration

Figure 3 illustrates the equilibrium behavior of ALP adsorption onto SSSAC at 30 °C, showing both (a) the adsorption capacity and (b) the percentage removal.

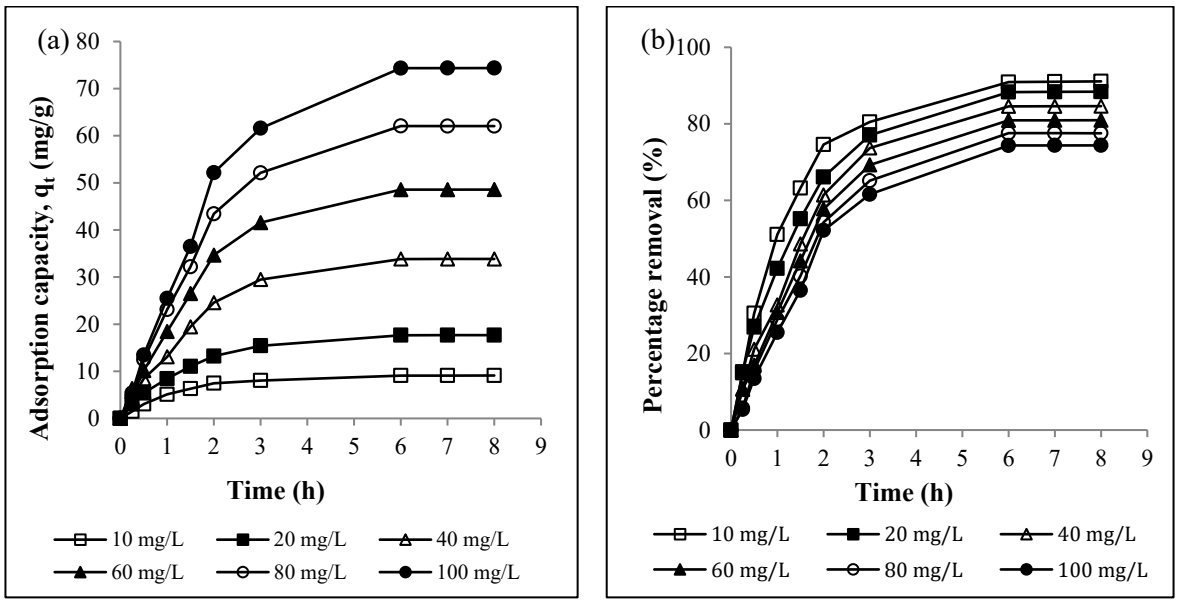

Figure 3: Equilibrium plots of (a) ALP uptakes and (b) ALP percentage removal versus time for different starting concentration at 30 °C

As seen in Figure 3(a), when the initial ALP concentration rises from 10 to 100 mg/L, the adsorption uptake increases markedly from 9.11 mg/g to 74.37 mg/g, indicating that more active sites become occupied with increasing solute concentration. However, Figure 3(b) demonstrates that the removal efficiency decreases from 91.10 % to 74.37 % as the concentration increases, suggesting that at higher ALP concentrations, the available adsorption sites become progressively saturated, leaving a smaller proportion of solute removed from solution. This inverse relationship between uptake and removal percentage is typical of adsorption systems where the driving force for mass transfer enhances total uptake but limits the relative removal efficiency once equilibrium is approached [11] .

3.2.2 The influence of ALP starting pH

Figure 4 presents the effect of pH on the adsorption capacity of SSSAC toward ALP at 30 °C. The adsorption capacity decreases steadily from 87.46 mg g^{-1} at pH 5 to 65.85 mg g^{-1} at pH 9, indicating that acidic conditions favor ALP uptake. The strong adsorption at low pH can be attributed to the relatively negative surface charge of SSSAC (as evidenced by the zeta potential value of −51.30 mV in Section 3.1.3). In contrast, ALP is a weak acid with a pKa of about 9.4 [19], and therefore remains predominantly non ionized (neutral) under acidic and near neutral conditions, while deprotonation begins as the pH approaches and exceeds its pKa, producing negatively charged species. As the pH increases, ALP progressively deprotonates to form anionic species, leading to electrostatic repulsion between the negatively charged adsorbent surface and the anionic drug molecules. This pH-dependent behavior is consistent with previous studies, where changes in functional group protonation and electrostatic interactions significantly influence adsorption performance [20]. Furthermore, the increased hydroxide ion concentration at higher pH competes with ALP for the same active sites, reducing adsorption efficiency [21]. The gradual decline in adsorption capacity with rising pH reflects this shift from attractive to repulsive interactions, suggesting that pH 5 is the most favorable condition for ALP removal. This behavior aligns with the amphoteric nature of ALP and the negatively charged surface characteristics of SSSAC, confirming that electrostatic forces play a significant role in the adsorption mechanism.

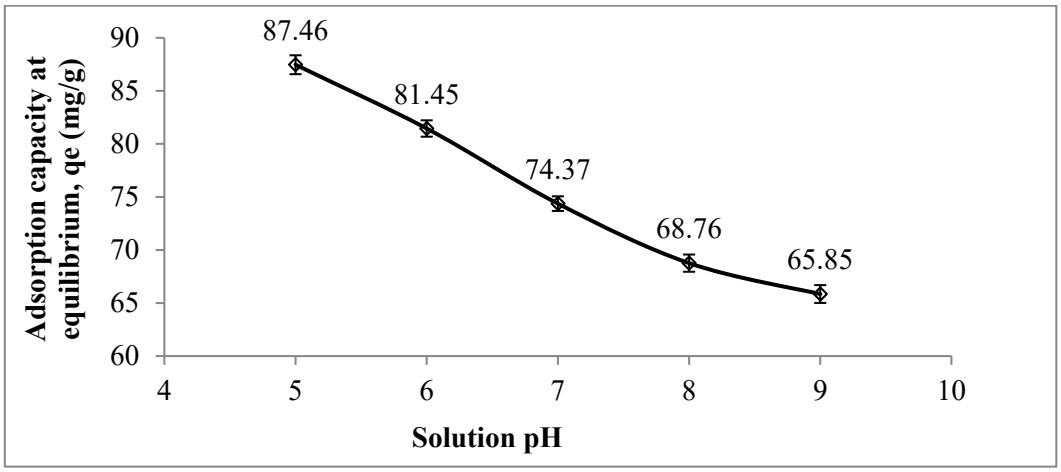

Figure 4: ALP uptakes plot under different pH at 30 °C

3.3 Adsorption isotherm

Figure 5 illustrates the adsorption isotherm plots, while Table 2 presents the corresponding isotherm parameters for the ALP-SSSAC system at 30 °C. Among all tested models, the Freundlich isotherm provided the best fit for the experimental data, signifying that ALP adsorption onto SSSAC follows a heterogeneous multilayer mechanism. This model exhibited the lowest RMSE value (1.15) and error percentage (5.52 %), confirming its superior predictive reliability compared to other models. The Freundlich constant n_F, obtained as 1.51, falls within the favorable adsorption range of $1 < n_F < 10$,

indicating efficient binding of ALP molecules onto the activated carbon surface [13]. This result implies that SSSAC contains a distribution of active sites with varying adsorption energies, thereby promoting multilayer uptake through diverse physicochemical interactions between ALP molecules and surface functional groups. This adsorption behavior is strongly supported by the BET analysis, which revealed a high surface area and well-developed mesoporosity, as well as the SEM observations showing a heterogeneous and porous surface structure, both of which are essential for accommodating multilayer adsorption.

Table 2: Isotherm parameters for ALP-SSSAC adsorption system at 30 °C

Isotherm models	Parameters	ALP-SSSAC
Langmuir	Q_m (mg/g)	113.84
	K_L (L/mg)	0.069
	RMSE	1.66
	Error (%)	7.69
Freundlich	n_F	1.72
	K_F (mg/g)(L/mg)$^{1/n}$	11.47
	$1/n_F$	0.58
	RMSE	1.15
	Error (%)	5.52
Temkin	A_T (L/mg)	1.31
	B_T (L/mg)	19.31
	RMSE	5.01
	Error (%)	21.00

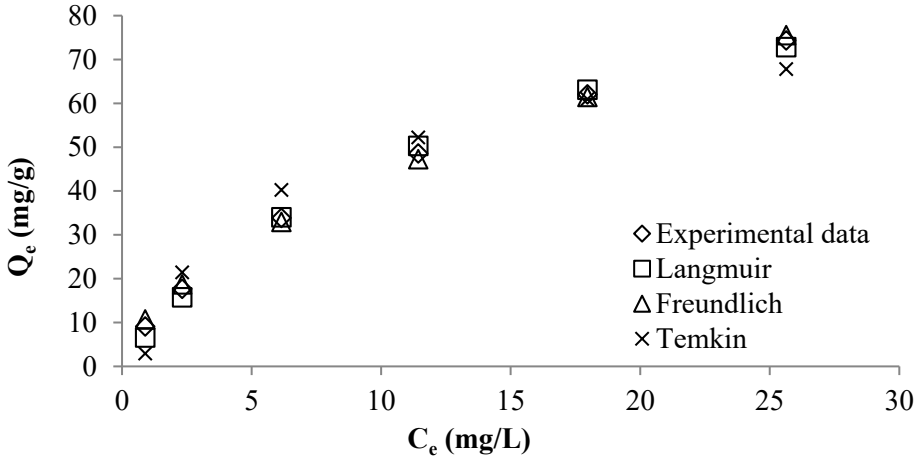

Figure 5: Isotherm plots for ALP-SSSAC adsorption system at 30 °C

3.4 Adsorption kinetic

Table 3 summarizes the kinetic parameters describing the adsorption of ALP onto SSSAC at 30 °C. The PFO model exhibited a significantly lower average error (6.02 %) compared with the PSO model (43.40 %), demonstrating better agreement between the calculated and experimental q_e values. This indicates that the adsorption kinetics are more appropriately described by the PFO model. The rate constant (k_1) decreased from 0.81 to 0.42 h^{-1} with increasing ALP concentration, suggesting that the adsorption rate slows as more surface sites become occupied and fewer readily accessible sites remain

available. In contrast, the PSO model produced significantly higher deviations, with q_e, calculated values greatly exceeding the experimental data, particularly at higher concentrations. This poor correlation indicates that chemisorption is not the dominant rate-limiting step in this system. Therefore, the kinetic results confirm that ALP adsorption onto SSSAC is mainly controlled by physisorption, involving diffusion and weak van der Waals interactions rather than chemical bonding [22]. This kinetic behaviour aligns well with the Freundlich isotherm findings, which described the adsorption as a multilayer process on a heterogeneous surface. Together, these results confirm that the ALP-SSSAC system involves rapid surface adsorption followed by multilayer physical interactions across sites of varying energy levels. This kinetic behavior is consistent with the morphological and textural characteristics observed in SEM and BET analyses, where the presence of interconnected pores and large surface area facilitates rapid diffusion and adsorption of ALP molecules onto the SSSAC surface.

Table 3: Kinetic parameters for ALP-SSSAC system at 30 °C

ALP starting concentration (mg/L)	q_e, actual (mg/g)	PFO			PSO		
		q_e, calculated	k_1 (h^{-1})	Error (%)	q_e, calculated	k_2 (g/mg.h)	Error (%)
10	9.09	9.08	0.81	0.11	11.22	0.0712	23.43
20	17.66	17.94	0.66	1.59	22.79	0.0273	29.05
40	33.83	35.97	0.53	6.33	48.42	0.0089	43.13
60	48.55	52.23	0.49	7.58	71.85	0.0053	47.99
80	62.06	67.80	0.45	9.25	95.83	0.0035	54.42
100	74.35	82.71	0.42	11.24	120.74	0.0024	62.39
		Average error (%)		**6.02**	**Average error (%)**		**43.40**

3.5 Regeneration results

The regeneration performance of SSSAC was evaluated for seven consecutive adsorption–desorption cycles using the combined solvent–alkaline method described earlier in Section 2.5. As illustrated in Figure 6, both adsorption capacity ($q_{e,n}$) and the remaining mass of regenerated SSSAC (m_n) exhibited gradual reductions with increasing regeneration cycles. The adsorption capacity decreased from 74.37 mg g^{-1} in the first cycle to 8.96 mg g^{-1} after the seventh cycle, corresponding to a decline of approximately 88 %. Similarly, the remaining mass of the adsorbent dropped from 100 % to 33.96 %, indicating continuous material loss during repeated regeneration. Accordingly, the weight loss, calculated using Eq. (10), increased progressively with cycle number, reaching a total loss of 66.04 % after the seventh cycle. The observed decline can be attributed to several concurrent factors. During each ethanol–water washing step, loosely bound ALP molecules and impurities were efficiently desorbed, but repeated washing may have also removed weakly attached surface fragments, contributing to gradual mass loss [23].

In the subsequent NaOH treatment, the alkaline medium facilitated the desorption of strongly adsorbed ALP via ionic exchange and disruption of π–π or hydrogen bonding interactions between ALP molecules and surface functional groups [24]. However, repeated exposure to NaOH could partially dissolve or hydrolyse oxygenated surface groups such as –COOH and –OH, leading to a progressive reduction in active adsorption sites and surface charge density [25]. The overall regeneration efficiency (RE_n) thus decreased steadily with each cycle, indicating that while the combined solvent–alkaline method was effective for initial recovery, the structural and chemical integrity of SSSAC was gradually compromised. After the fifth cycle, a more pronounced decline in $q_{e,n}$ was evident, suggesting partial pore collapse or carbon framework weakening due to repeated solvent swelling and alkaline reactions. Despite this reduction, SSSAC retained about 70 % of its initial adsorption capacity after the third cycle, demonstrating that the adsorbent maintained reasonable reusability for at least three operational cycles before significant deterioration occurred.

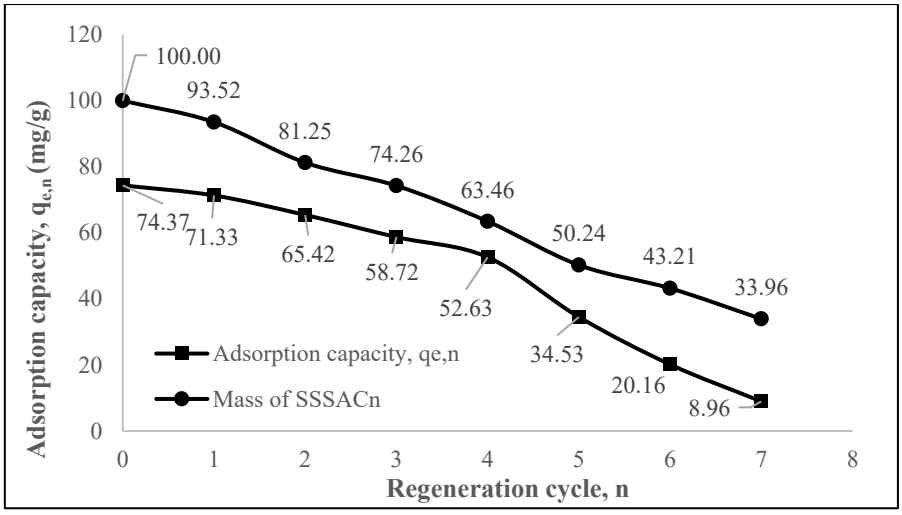

Figure 6: Regeneration plots for ALP-SSSAC adsorption system at 30 °C

4. CONCLUSIONS

This study confirmed that sunflower seed shells can be efficiently transformed into SSSAC for the adsorption of ALP from aqueous solutions. The KOH activation process successfully enhanced the textural and surface charge properties, converting the dense precursor into a highly porous adsorbent with a zeta potential of −51.30 mV. This enhancement is supported by BET analysis, which revealed a significant increase in surface area and pore volume, and SEM observations showing the development of a well-defined porous structure, both of which contribute to improved adsorption performance. The adsorption performance was influenced by the initial ALP concentration and solution pH, with the optimum uptake of 87.54 mg/g achieved at pH 5. This behavior is consistent with the electrostatic interaction between ALP species and the negatively charged adsorbent surface. The Freundlich isotherm best represented the equilibrium data, indicating a multilayer adsorption mechanism on a heterogeneous surface, while the Langmuir model estimated a Q_m value of 113.84 mg/g. Kinetic analysis showed that the PFO model provided the best fit, implying that the process was primarily governed by physisorption. Regeneration studies demonstrated that SSSAC maintained satisfactory performance up to the fifth cycle, after which the ALP uptake dropped to 34.53 mg/g and the adsorbent yield reduced to about 50 %. Therefore, reactivation beyond the fifth cycle is not recommended due to excessive structural and mass loss. For future work, modification of SSSAC using mild oxidizing agents or surface functionalization is suggested to enhance its regeneration stability.

Acknowledgements

This research is supported by Malaysian Ministry of Higher Education under the Prototype Research Grant Scheme (project code: PRGS/1/2025/TK/USM/01/1).

Author Contributions

All authors contributed toward data analysis, drafting and critically revising the paper and agree to be accountable for all aspects of the work.

Disclosure of Conflict of Interest

The authors have no disclosures to declare.

Compliance with Ethical Standards

The work adheres to the ethical standards, ensuring that all experimental procedures and methodologies were conducted with integrity and respect for ethical guidelines.

References

[1] Jordan, A. & Gresser, U. (2018). Side effects and interactions of the xanthine oxidase inhibitor febuxostat. *Pharmaceuticals,* 11(2), 51.

[2] Munzhelele, E. P., Mudzielwana, R., Wasiu, A. & Gitari, W. (2024). Pharmaceutical contaminants in wastewater and receiving water bodies of south africa: a review of sources, pathways, occurrence, effects, and geographical distribution. *Water,* 16, 796.

[3] Funke, J., Prasse, C., Lütke , E. C. & Ternes, T. A. (2015). Oxypurinol – A novel marker for wastewater contamination of the aquatic environment. *Water Research,* 74, 257-265.

[4] Yang, C., Zheng, Q., Wang, Z., Ahmed, F., Tscharke, B., Yang, S., O'Brien, J. W., Verhagen, R., Mueller, J. F., Tong, L. & Thai, P. K. (2025). Occurrence and emission evaluation of Oxypurinol and Metformin from effluent in WWTPs across Australia. *Environmental Science & Technology,* 59(23), 11767-11775.

[5] Mohamad, F. M. Y., Rashid, M. M., Alam, M. M. & Ahmad, M. A. (2025). Copper metal-functionalized carbon from rattan waste via microwave pyrolysis for enhanced chloramphenicol removal: Optimization and F-test study. *Particuology,* 100, 196-213.

[6] Yusop, M. F. M., Erniza, M. J. J., Din, A. T. M., Bello, O. S. & Ahmad, M. A. (2022). Single-stage optimized microwave-induced activated carbon from coconut shell for cadmium adsorption. *Chemical Engineering & Technology,* 45(11), 1943-1951.

[7] Yusop, M. F. M., Rashid, M. M., Alam, M. M. & Ahmad, M. A. (2026). Optimized copper-functionalized carbon from Lansium parasiticum trunk for chloramphenicol removal from aqueous solution. *International Journal of Environmental Science and Technology,* 23(4), 306.

[8] De, S. J., Arauzo, P. J. & Ronsse, F. (2025). Molten salts vs conventional activating agents for activated carbon production: A comprehensive review. *Journal of Analytical and Applied Pyrolysis,* 192, 107239.

[9] Casoni, A. I., Gutierrez, V. S. & Volpe, M. A. (2019). Conversion of sunflower seed hulls, waste from edible oil production, into valuable products. *Journal of Environmental Chemical Engineering,* 7(1), 102893.

[10] Guo, J. & Lua, A. C. (1999). Textural and chemical characterisations of activated carbon prepared from oil-palm stone with H_2SO_4 and KOH impregnation. *Microporous and Mesoporous Materials,* 32(1), 111-117.

[11] Mohamad, F. M. Y., Abdullah, A. Z. & Ahmad, M. A. (2023). Adsorption of remazol brilliant blue R dye onto jackfruit peel based activated carbon: Optimization and simulation for mass transfer and surface area prediction. *Inorganic Chemistry Communications,* 158, 111721.

[12] Yusop, M. F. M., Rashid, M. M., Alam, M. M. & Ahmad, M. A. (2026). Cu^{2+}-Surface-Modified Activated Carbon from Nutshells for Enhanced Metformin Removal: Mass Transfer Simulation, Attraction Mechanism and F-Test Studies. *Water, Air, & Soil Pollution,* 237(9), 518.

[13] Liu, C., Yan, X., Zhang, H. X., Yang, J. M. & Yoon, K. B. (2024). Biochars and modified-biochars for toxic-metal/metalloid ions sorption in various mixed solution systems: A review on kinetic and isotherm models. *Desalination and Water Treatment,* 319, 100404.

[14] Firdaus, M. Y. M., Rashid, M. M., Alam, M. M. & Ahmad, M. A. (2025). Enhanced Cd^{2+} removal via deprotonated-mango trunk functionalized carbon: Optimization and F-test for linear and non-linear isotherm and kinetic models. *Chemical Engineering Research and Design,* 220, 96-116.

[15] Revellame, E. D., Fortela, D. L., Sharp, W., Hernandez, R. & Zappi, M. E. (2020). Adsorption kinetic modeling using pseudo-first order and pseudo-second order rate laws: A review. *Cleaner Engineering and Technology,* 1, 100032.

[16] Yusop, M. F. M., Baharudin, M. H., Rashid, M. M., Alam, M. M. & Ahmad, M. A. (2025). Amoxicillin adsorption onto oil palm trunk-derived activated carbon: synthesis optimization, modelling of mass transfer and ultrasonic regeneration. *Journal of Chemical Technology & Biotechnology,* 100(6), 1310-1327.

[17] Ma, R., Fu, G., Ai, L., Xu, M., Guo, N. & Wang, L. (2025). A low dose KOH activation method is used to prepare starch-based porous carbon for high performance supercapacitors. *International Journal of Biological Macromolecules,* 307, 142320.

[18] Park, S. J. & Jung, W. Y. (2002). Effect of KOH Activation on the Formation of Oxygen Structure in Activated Carbons Synthesized from Polymeric Precursor. *Journal of colloid and interface science,* 250, 93-8.

[19] Deng, L., Li, Y., Feng, F., Wu, D. & Zhang, H. (2019). Encapsulation of allopurinol by glucose cross-linked gelatin/zein nanofibers: Characterization and release behavior. *Food Hydrocolloids,* 94, 574-584.

[20] Firdaus, M. Y. M., Rashid, M. M., Alam, M. M. & Ahmad, M. A. (2025). Synthesis of deprotonated grape stem functionalized carbon for boosted Cu^{2+} adsorption – Optimization, interaction mechanism, and F-test analysis. *Microchemical Journal,* 218, 115795.

[21] Mohamad, Y. M. F., Abdullah, A. Z. & Ahmad, M. A. (2024). Amoxicillin adsorption from aqueous solution by Cu(II) modified lemon peel based activated carbon: Mass transfer simulation, surface area prediction and F-test on isotherm and kinetic models. *Powder Technology,* 438, 119589.

[22] Wang, J. & Guo, X. (2023). Adsorption kinetics and isotherm models of heavy metals by various adsorbents: An overview. *Critical Reviews in Environmental Science and Technology,* 53(21), 1837-1865.

[23] Alsawy, T., Rashad, E., El-Qelish, M. & Mohammed, R. H. (2022). A comprehensive review on the chemical regeneration of biochar adsorbent for sustainable wastewater treatment. *npj Clean Water,* 5(1), 29.

[24] Sporsho, S. S., Saha, D., Khan, M. H., Rahman, M. S., Rukh, M., Islam, M. R., Chakma, T., Haque, F., Roy, H., Sarkar, D. & Islam, M. S. (2025). Insights into adsorbent-based pharmaceutical wastewater treatment and future developments toward sustainability. *RSC Advances,* 15(59), 50597-50632.

[25] Dai, Y., Zhang, N., Xing, C., Cui, Q. & Sun, Q. (2019). The adsorption, regeneration and engineering applications of biochar for removal organic pollutants: A review. *Chemosphere,* 223, 12-27.